Scaling properties of force networks for compressed particulate systems

L. Kovalcinova, A. Goullet, and L. Kondic

Phys. Rev. E **93**, 042903 — Published 15 April 2016

DOI: 10.1103/PhysRevE.93.042903

Scaling Properties of Force Networks for Compressed Particulate Systems

L. Kovalcinova, A. Goullet, and L. Kondic
Department of Mathematical Sciences,
New Jersey Institute of Technology,
University Heights, Newark, NJ 07102

We consider, computationally and experimentally, the scaling properties of force networks in the systems of circular particles exposed to compression in two spatial dimensions. The simulations consider polydisperse and monodisperse particles, both frictional and frictionless, and in experiments we use monodisperse and bidisperse frictional particles. While for some of the considered systems we observe consistent scaling exponents describing the behavior of the force networks, we find that this behavior is *not universal*. In particular, we find that frictionless systems, independently of whether they partially crystallize under compression or not, show scaling properties that are significantly different compared to the frictional disordered ones. The findings of non-universality are confirmed by explicitly computing fractal dimension for the considered systems. The results of the physical experiments are consistent with the results obtained in simulations of frictional disordered systems.

PACS numbers: 45.70.-n, 89.75.Da

I. INTRODUCTION

Particulate materials are relevant in a variety of systems of practical relevance. It is well known that macroscopic properties of these systems are related to the force networks - the mesoscale structures that characterize the internal stress distribution. The force networks are built on top of the contact networks formed by the particles. These contact networks have been studied using a number of approaches, see [1, 2] for reviews. However, the properties of force networks, that form a subset of the contact networks based on the interaction force, are not slaved to the contact one: a single contact network can support infinite set of possible force networks, due to indeterminacy of the interaction forces. These force networks have been analyzed using a variety of approaches, including distributions of the force strengths between the particles [3, 4], the tools of statistical physics [5–8], local properties of the force networks [9–11], networks-based type of analysis [12–14], as well as the topology-based measures [15, 16]. Of relevance to the present work are the recent results obtained using algebraic topology [17–19] that have shown that in particular frictional properties of the particles play an important role in determining connectivity properties of the considered force networks. For illustration, Fig. 1 shows an example of the experimental system (discussed in more details later in the paper), where the particles are visualized without (a) and with (b) cross-polarizers; in the part (b) force networks are clearly visible.

The recent work [20] suggests that properties of these force networks are universal. In other words, the finding is that, when properly scaled, the distributions of force clusters (defined as groups of particles in contact experiencing the force larger than a specified threshold) collapse to a single curve. In [20] it has been argued that this universality finding is independent of the particle properties like polydispersity and friction, or anisotropy of the force networks induced by shear [21]. The influence of anisotropy on the exponents describing scaling (and universality) properties of force networks was further considered using q-model [22], where it was found that anisotropy may have a strong influence on the scaling exponents.

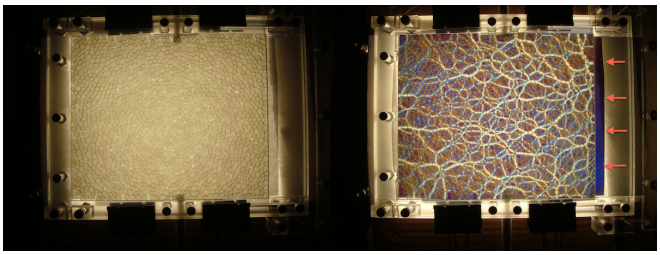

(a) (b)

FIG. 1: (Color online) Experimental images of a two-dimensional system of photoelastic particles, obtained (a) without and (b) with cross-polarizer. The arrows indicates the side of the container where pressure is applied.

In the present work, we further explore the generality of the proposed universality, using discrete element simulations in the setup where anisotropy is not relevant. This exploration is motivated in part by the following 'thought' experiment. Consider a model problem of perfectly ordered monodisperse particles that under compression form a crystal-like structure. In such a structure, each particle experiences the same total normal force, $F = 1$ (normalized by the average force). If we choose any force threshold $\bar{F} \leq 1$, we obtain only one (percolating) cluster that includes all the particles. For any $\bar{F} > 1$, there are no particles. As an outcome, the mean cluster size, $\bar{S}(\bar{F})$ (including the percolating cluster), is a Heaviside function regardless of the system

size and $S(\bar{F})$, that is a mean cluster size without the percolating cluster, is zero everywhere. Considering the scaling properties of the S-curve for different system sizes is therefore trivial and the scaling exponents (discussed in detail in the rest of the paper) are not well defined. Furthermore, the fractal dimension, D_f, related to the scaling exponents [23], leads trivially to $D_f = D$, where D is the number of physical dimensions. Clearly, the scaling properties of such an ideal system are different compared to the ones expected for a general disordered system. Therefore, we found at least one system where 'universality' does not hold.

One could argue that such perfect system as discussed above is not relevant to physical setups, so let us consider a small perturbation - for example a system of particles of the same or similar sizes, possibly frictionless, that are known to partially crystallize under compression [17, 18]. For such systems, $\bar{S}(\bar{F})$ is not a Heaviside step function, but it may be close to it. Therefore, there is an open question whether these systems (that partially crystallize) still lead to 'universal' force networks. One significant result of this work is that this is not the case. Going further, we will also show that the systems of frictionless particles, even if they do not crystallize partially, still lead to non-universal force networks.

The remaining part of this paper is organized as follows. In Sec. II we describe the simulations that were carried out. We then follow by the main part of the paper, Sec. III, where we describe computations of scaling parameters in Sec. III A; discuss the results for the scaling exponent, ϕ, and the fractal dimension, D_f, in Sec. III B; outline the influence of the structural properties of considered systems in Sec. III C; discuss the influence of compression rate and different jamming packing fractions in Sec. III D, and then present the results for the other scaling parameters, ν and f_c in Sec. III E. We conclude this Section by presenting the results of physical experiments that were motivated by the computational results in Sec. III F. Section IV is devoted to the conclusions.

II. SIMULATIONS

We perform discrete element simulations using a set of circular particles confined in a square domain, using a slow-compression protocol [17, 18, 24], augmented by relaxation as described below. Initially, the system particles are placed on a square lattice and are given random velocities; we have verified that the results are independent of the distribution and magnitude of these initial velocities. Gravitational effects are not included; we also ignore the interaction of the particles with the substrate in the simulations (substrate is present in the experiments as illustrated in Fig. 1; these effects will be discussed elsewhere). The discussion related to possible development of spatial order as the system is compressed can be found in [18], and will be discussed in more detail later. In [24] it was shown that the considered systems are spatially isotropic, that is, 4-fold symmetry imposed by the domain shape does not influence the results.

In our simulations, the diameters of the particles are chosen from a flat distribution of the width r_p. System particles are soft inelastic disks and interact via normal and tangential forces, including static friction, μ (as in [17, 18, 24]). The particle-particle (and particle-wall) interactions include normal and tangential components. The normal force between particles i and j is

$$\begin{aligned} \mathbf{F}_{i,j,n} &= k_n x \mathbf{n} - \gamma_n \bar{m} \mathbf{v}^n_{i,j} \\ r_{i,j} = |\mathbf{r}_{i,j}|, \quad \mathbf{r}_{i,j} &= \mathbf{r}_i - \mathbf{r}_j, \quad \mathbf{n} = \mathbf{r}_{i,j}/r_{i,j} \end{aligned} \tag{1}$$

where $\mathbf{v}^n_{i,j}$ is the relative normal velocity. The amount of compression is $x = d_{i,j} - r_{i,j}$, where $d_{i,j} = (d_i + d_j)/2$, d_i and d_j are the diameters of the particles i and j. All quantities are expressed using the average particle diameter, d_{ave}, as the length scale, the binary particle collision time $\tau_c = 2\pi\sqrt{d_{ave}/(2gk_n)}$ as the time scale, and the average particle mass, m, as the mass scale. $\bar{m}$ is the reduced mass, k_n (in units of mg/d_{ave}) is set to a value corresponding to photoelastic disks [25], and γ_n is the damping coefficient [26]. The parameters entering the linear force model can be connected to physical properties (Young modulus, Poisson ratio) as described e.g. in [26].

We implement the commonly used Cundall-Strack model for static friction [27], where a tangential spring is introduced between particles for each new contact that forms at time $T = T_0$. Due to the relative motion of the particles, the spring length, $\boldsymbol{\xi}$, evolves as $\boldsymbol{\xi} = \int_{T_0}^{T} \mathbf{v}^t_{i,j}\,(T')\,dT'$, where $\mathbf{v}^t_{i,j} = \mathbf{v}_{i,j} - \mathbf{v}^n_{i,j}$. For long lasting contacts, $\boldsymbol{\xi}$ may not remain parallel to the current tangential direction defined by $\mathbf{t} = \mathbf{v^t_{i,j}}/|\mathbf{v^t_{i,j}}|$ (see, e.g,. [28]); we therefore define the corrected $\boldsymbol{\xi}' = \boldsymbol{\xi} - \mathbf{n}(\mathbf{n}\cdot\boldsymbol{\xi})$ and introduce the test force

$$\mathbf{F}_{t*} = -k_t \boldsymbol{\xi}' - \gamma_t \bar{m} \mathbf{v}^t_{i,j} \tag{2}$$

where γ_t is the coefficient of viscous damping in the tangential direction (with $\gamma_t = \gamma_n$). To ensure that the magnitude of the tangential force remains below the Coulomb threshold, we constrain the tangential force to be

$$\mathbf{F}_t = min(\mu|\mathbf{F}_n|, |\mathbf{F}_{t*}|)\mathbf{F}_{t*}/|\mathbf{F}_{t*}| \tag{3}$$

and redefine $\boldsymbol{\xi}$ if appropriate.

The simulations are carried out by slowly compressing the domain, starting at the packing fraction 0.63 and ending at 0.90, by moving the walls built of L monodisperse particles with diameters of size d_{ave} placed initially at equal distances, d_{ave}, from each other. The wall particles move at a uniform (small) inward velocity, v_c, equal to $v_0 = 2.5 \cdot 10^{-5}$ (in units of d_{ave}/τ_c). Due to compression and uniform inward velocity, the wall particles (that do not interact with each other) overlap by a small amount. When the effect of compression rate is explored, the compression is stopped to allow the system to relax.

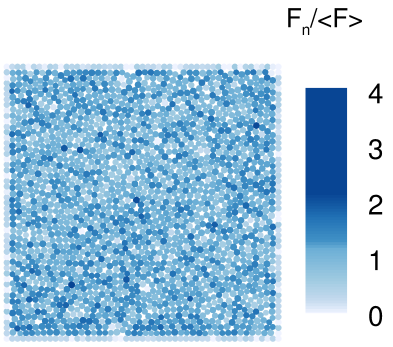

FIG. 2: (Color online) Reference system at $\rho = 0.9$.

In order to obtain statistically relevant results, we simulate a large number of initial configurations (typically 120), and average the results.

We integrate Newton's equations of motion for both the translation and rotational degrees of freedom using a 4th order predictor-corrector method with time step $\Delta T = 0.02$. Our reference system is characterized by $k_n = 4 \cdot 10^3$, $e_n = 0.5$, $\mu = 0.5$, and $k_t = 0.8k_n$ [29]; the particles are polydisperse with $r_p = 0.2$ and if not specified otherwise, it is assumed that $L = 50$ with the total of $N_p \approx 2000$ particles. Larger domain simulations are carried out with N_p up to $\approx 10,000$. Since the focus of the present work is on exploring universality of the force network, we have not made any particular effort to match the parameters between the simulations and the experiments discussed in Sec. III F.

III. FORCE NETWORKS AND SCALING LAWS

In earlier work [24], we discussed the percolation and jamming transitions that take place as the system is exposed to compression. We identified the packing fractions at which these transitions occur as ρ_c (percolation) and ρ_J (jamming). For the present purposes, the most relevant finding is that for the repulsive systems, ρ_c and ρ_J are very close and, in the limit of quasi-static compression, the two transitions coincide and $\rho_c = \rho_J$. In this paper we focus on the systems such that $\rho > \rho_c$, and in particular on the properties of the force networks. Figure 2 shows an example of a compressed packing, with the particles color coded according to the total normal force, F_n, normalized by the average normal force, $< F >$ (we will focus only on the normal forces in the present work). The properties of these networks depend on the force threshold, $\bar{F}$, such that only the particles with $\bar{F} \leq (F_n/ < F >)$ are included. We will now proceed to use the tools of percolation theory to study cluster size distribution and mean cluster size as $\bar{F}$ varies, considering force networks to be composed of the particles and inter-particle forces that can be thought of as nodes and bonds, consecutively.

We start by introducing the cluster number, n_s, representing the average (over all realizations) number of clusters with s particles; note that n_s depends on ρ and $\bar{F}$. From the percolation theory [23], we know that n_s at the percolation force threshold, f_p, can be characterized by the following scaling law

$$n_s \propto s^{-\tau}, \tag{4}$$

with the Fisher exponent τ. The percolation force threshold, f_p, is defined here as the one for which percolation probability is larger than 0.5, as in [24].

Using n_s, we can define the mean cluster size, $S(\bar{F})$, as

$$S(\bar{F}) = \frac{\sum_s' s^2 n_s}{\sum_s' s n_s} \tag{5}$$

where $\sum_s'$ denotes the sum over the non-percolating clusters of size s.

The scaling law for the mean cluster size, $S(\bar{F})$, is according to [23] given by

$$S(\bar{F}) = A\, N^{\phi} \mathcal{M}_2 \left(B\, (\bar{F} - f_c) N^{\frac{1}{2\nu}} \right), \tag{6}$$

where A, B are the coefficients independent of the system size, ϕ, ν are two critical exponents with $\phi = (3 - \tau)/(\tau - 1)$ and f_c is a critical force threshold found from collapse of rescaled S curves as described later. Note that f_p and f_c do not necessarily agree; we will discuss this issue later in the text. Here, N is the total number of contacts in the system, (excluding the contacts with the wall particles), and $\mathcal{M}_2(\cdot)$ is the second moment of the probability distribution of cluster size s. The question is whether there is an universal set of parameters ϕ, ν such that the $S(\bar{F})N^{-\phi}$ curves obtained for different systems, collapse onto a single curve.

A. Computing the scaling parameters

To find the exponents ϕ, ν and the parameter f_c, we follow the procedure similar to the one described in [20]. For a given simulation, we find the cluster number, n_s, for cluster size, s, ranging from $s = 1$ up to $s = N_p$, given a force threshold $\bar{F}$. The cluster search is performed over the range $\bar{F} \in [0, 5]$ with 501 discrete levels. Then, the mean cluster size, $S(\bar{F})$, is computed using Eq. (5). The computation of n_s and $S(\bar{F})$ is performed for the systems characterized by (wall length) $L = 25,\ 50,\ 75$, and 100, and for the discrete set of ρ's, such that $\rho > \rho_c$.

Figure 3(a) (top) shows an example of our results for $S(\bar{F})$ for various L's for the reference system at $\rho = 0.9$, averaged over 120 realizations. As expected, the magnitude of the peak of $S(\bar{F})$ is an increasing function of L: according to percolation theory [23], $S \propto L^{\beta}$, $\beta > 0$ at the percolation threshold. We note from Fig. 3(a)

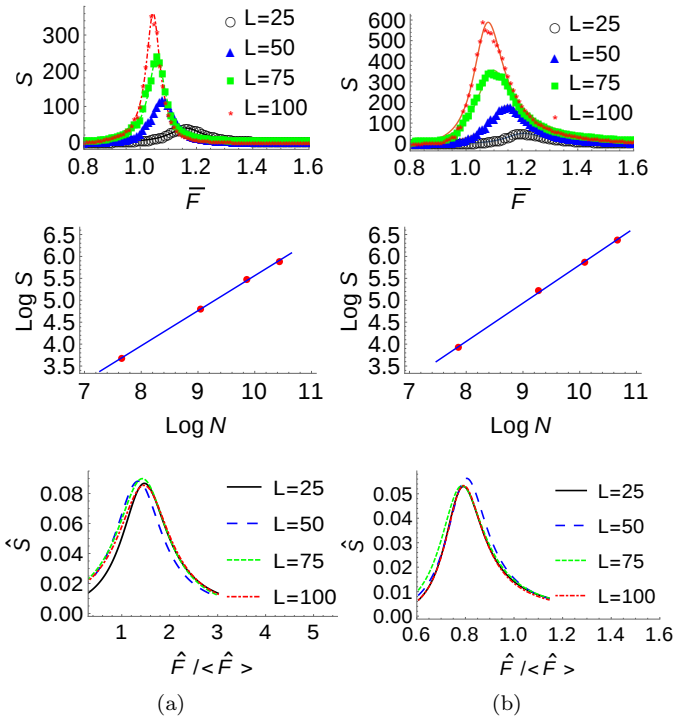

FIG. 3: (Color online) (a) Reference and (b) $r_p = 0.0, \mu = 0.0$ system at $\rho = 0.9$ showing (top to bottom) mean cluster size S; magnitude of the peak of S versus the total number of contacts, N, for different system sizes, L; and collapse of the rescaled curves, $\hat{S}$ vs. force threshold, $\hat{F}$, normalized by the rescaled average force, $< \hat{F} >$ (see the text for definitions of the rescaled quantities). Note different range of axes in (a) and (b).

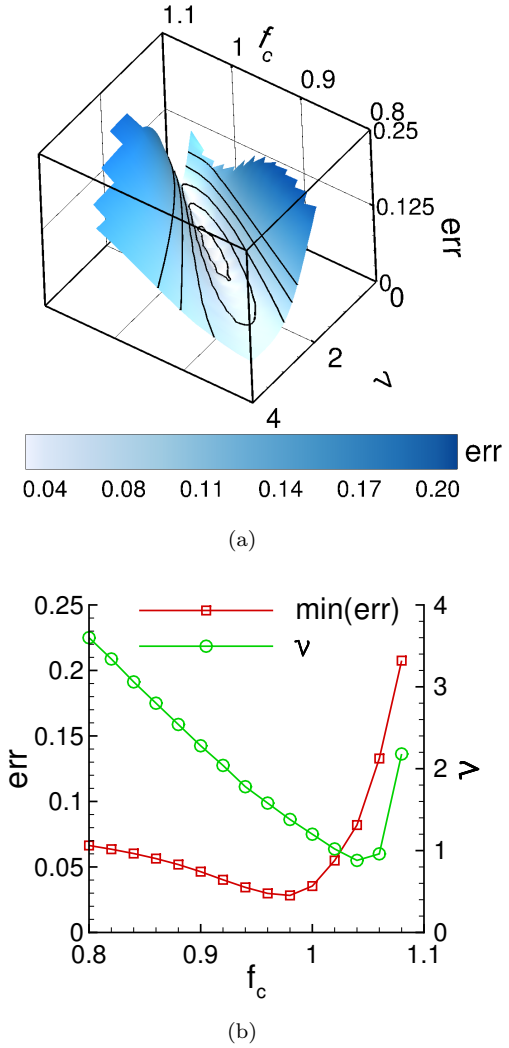

FIG. 4: (Color online) Error plot for the reference system at $\rho = 0.9$: (a) *err* as a function of f_c and ν; the black lines are slices through different values of *err* and (b) minimum of *err* (red line with squares) as a function of f_c; here for each f_c value we choose ν that minimizes *err*; the used values of ν are shown by the green line with circles.

(top) that f_p (corresponding to the peak of the $S(\bar{F})$ curves [23]) is a decreasing function of L. For all systems and system size considered in the present work, the values of f_p are in the range $[1.05, 1.25]$.

From the magnitude of the peaks of $S(\bar{F})$, one can determine the optimal critical exponent ϕ; for $\mathcal{M}_2$ to be a "universal" curve regardless of the system size, $N^{-\phi}$ and $S(\bar{F})$ have to balance each other as L varies. The exponent ϕ is obtained from the linear regression through the peaks of $\log S(\bar{F})$ as a function of $\log N$. Figure 3 (middle) shows the values of peaks as a function of N in a log-log scale and a fit leading to a value of $\phi = 0.80 \pm 0.03$ within the 95% confidence interval.

Using the optimal value for ϕ, the remaining two parameters, f_c and ν, are determined by attempting to collapse the average $S(\bar{F})$ curves, such as the ones shown in Fig. 3 (top), around the maxima. We define the (large) range of values of f_c and ν over which the search is carried out: $f_c \in [0.5, 2.5], \nu \in [0.5, 14]$ with a discretization step 10^{-2}. The search range for both parameters is chosen in a way such that we always find optimal values of f_c and ν; we verified that our results do not change if we assume larger range. For each L, we find the interval of force thresholds, $\bar{F} \in [a_L, b_L]$, for which $S(\bar{F}) \geq S_{\max}/8$, where $S_{\max} = \max\{S(\bar{F})\}$. The results are not sensitive to this specific choice of a_L and b_L. For each pair f_c, ν we take the common subinterval $[a', b'] = \cap[a'_L, b'_L]$ where $a'_L = (a_L - f_c)N^{1/(2\nu)}, b'_L = (a_L - f_c)N^{1/(2\nu)}$ are rescaled endpoints of the interval $[a_L, b_L]$.

The optimal values of f_c and ν are found by minimizing the error, *err*, defined by

$$err = \frac{1}{M} \sum_{m<n} \sum_{i=0}^{M-1} \left| \hat{S}_{L_m}(\hat{F}_i) - \hat{S}_{L_n}(\hat{F}_i) \right| . \quad (7)$$

(8)

Here $L_m, L_n \in \{25, 50, 75, 100\}$ are different system

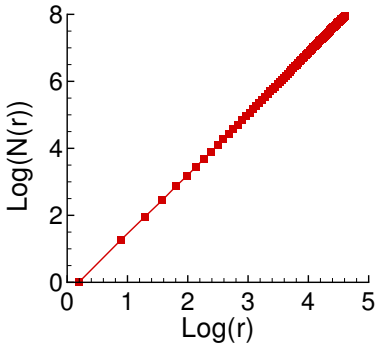

FIG. 5: (Color online) Number of subdomains covering the percolating cluster, $\mathcal{N}(r)$, as a function of the distance, r in log-log scale for the reference case at $\rho = 0.9$.

sizes, $\hat{F}_i = \bar{F}_i N^{-1/(2\nu)} + f_c$ and $\hat{S}_{L_m}(\hat{F}_i) = S_{L_m}(\hat{F}_i N^{-\phi})$. We choose $\hat{F}_i = a' + i d_F$ with discretization step $d_F = (b' - a')/(M-1)$ and $i = 0 \ldots (M-1)$ with total of $M = 100$ discretization points.

Note that the expression for err does not depend on the size of the interval over which the collapse of the curves is attempted.

Figure 3 (bottom) shows the collapse of the S curves as a function of the rescaled force threshold normalized by the average force threshold, $\hat{F}/ < \hat{F} >$; visual inspection suggests that indeed a good collapse was found and we continue by discussing the error using the optimal values of f_c, ν.

Figure 4(a) plots the contour of err as a function of f_c and ν for the reference system at $\rho = 0.9$. More precise information can be reached from Fig. 4(b) that shows err and ν, that minimizes err, as a function of f_c. We find that err reaches a well defined minimum at $f_c \approx 0.98$ for $\nu \approx 1.38$.

B. The scaling exponent ϕ and the fractal dimension

Before discussing how the results for ϕ, ν, and f_c depend on the properties of the particles, we mention an alternative approach to compute ϕ. According to [23], ϕ is related to the fractal dimension, D_f, of the percolating cluster at the percolation threshold, f_p, as $1 + \phi = D_f$. We compute D_f from the mass of the percolating cluster, using the Minkowski-Bouligand (or box counting) method. For each realization and each ρ, we divide the domain into square sub-domains of the size r, with r ranging from particle size up to L (≈ 500 discretization steps are used). The number of sub-domains/squares, $\mathcal{N}(r)$, that we need in order to cover the area occupied by the percolating cluster scales as

$$\mathcal{N}(r) \sim r^{D_f}. \qquad (9)$$

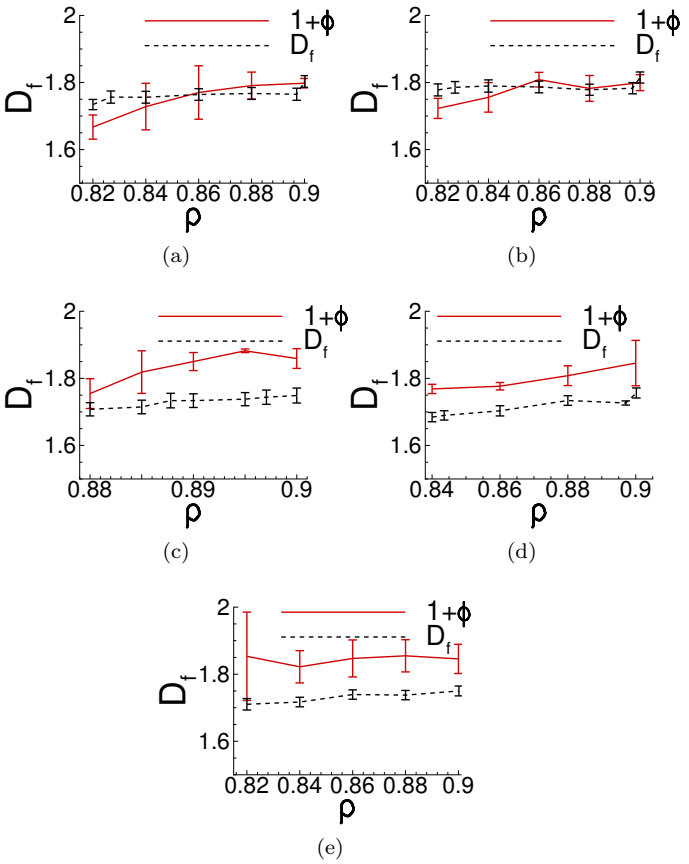

FIG. 6: (Color online) Fractal dimension, D_f, and scaling exponent $1 + \phi$ as a function of ρ: (a) $r_p = 0.0$, $\mu = 0.5$ (b) $r_p = 0.2$, $\mu = 0.5$ (reference system) (c) $r_p = 0.0$, $\mu = 0.0$, (d) $r_p = 0.2$, $\mu = 0.0$ and (e) $r_p = 0.4$, $\mu = 0.0$. For D_f, the error bars represent standard error; for ϕ, the error bars are derived from the accuracy of the fit, as explained in the text. The jamming packing fractions for the considered systems are $\rho_J =$ 0.804, 0.789, 0.861, 0.827 and 0.805, respectively [24].

To have a sufficiently large r, we compute D_f for the largest system size considered, with $L = 100$. Figure 5 shows r and $\mathcal{N}(r)$ in a log-log scale for the reference case and for $\rho = 0.9$ and $L = 100$. We find a good fit with $D_f = 1.783 \pm 0.016$. The value of D_f is computed as an average slope over 120 realizations and the error on D_f is computed as standard deviation.

For the present case, we find that D_f and ϕ are consistent; it is encouraging to see that the two independent procedures lead to the consistent results. Note also that the error in D_f is smaller than the one for ϕ; this is due to the fact that D_f is based on the properties of the percolating cluster that typically involves large number of particles, while the calculation of ϕ is based on smaller clusters. Therefore, the quality of data used for calculating D_f is in general much better.

We note that the values obtained for ϕ are significantly lower than those given in [20] (reported value $\phi \sim 0.9$), which is outside of the confidence interval for ϕ and D_f computed here. While it is difficult to comment on the source of this difference, it may have to do with the manner in which ϕ is computed in [20] - only a single domain size with $\approx 10,000$ particles was used, and then this domain was split into subdomains, with the largest subdomains discarded. The remaining subdomains contain relatively small number of particles, leading to potential inaccuracy of the results.

Figure 6 shows the independently computed values for ϕ and D_f for the systems considered, and for the packing fractions above jamming, $\rho > \rho_J$; note that each of the considered systems (that differ by frictional properties and polydispersity) jams at different ρ_J, listed in the caption of Fig. 6. Figure 6(a) shows that for the reference system, D_f and $1+\phi$ are in general consistent for all ρ's considered, with slightly larger discrepancies close to ρ_J.

Figure 6(b) shows the results for D_f and $1+\phi$ for the $r_p = 0.0,\ \mu = 0.5$ system. Similarly as for the reference case, the values of $1+\phi$ and D_f are consistent (the results for ϕ and D_f, together with the values of ν and f_c are also given in Tables I and II). However, for the frictionless systems, shown in Fig. 6(c - e), we find that there is a notable discrepancy between $1+\phi$ and D_f. By comparing frictional and frictionless results, we note that the discrepancy comes from considerably smaller values of D_f for the frictionless ones. This is significant, since D_f can be computed very accurately for all packing fractions, showing clearly strong influence of friction on the fractal dimension.

C. Influence of the friction and particle structure on the properties of force networks

The obvious question is what is the source of such a large difference between frictional and frictionless systems? Is it the partial crystallization that may occur for frictionless systems, or the differences in underlying force networks that are independent of the geometric order? We note that the issue of the connection between the properties of force networks, inter-particle friction and particle ordering was considered in the literature on the level of force probability density function, see, e.g. [6, 30, 31] and also studied by using persistence analysis [18]; the influence of friction on jamming transition was considered as well, see, e.g. [24, 32–34]. In the present context, the results given in this and the preceding section show that, in fact, friction itself (and not packing structure alone) is responsible for the breakup of universality.

We proceed by discussing the influence of friction and polydispersity on the structural properties of the considered systems. To start with, we focus on the level of crystallization in frictionless and frictional systems. For the largest packing fraction, $\rho = 0.9$, for all considered

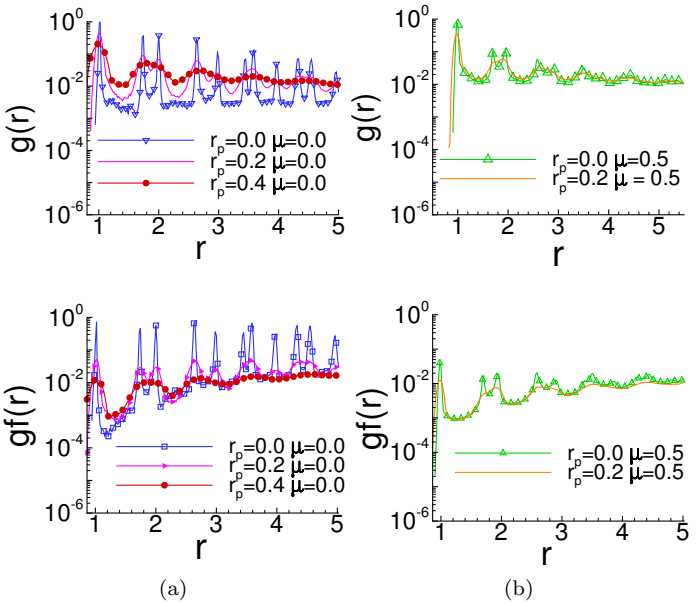

FIG. 7: (Color online) Pair correlation function, $g(r)$, and force correlation function, $g_f(r)$, at $\rho = 0.9$ for (a) frictionless systems, and (b) frictional systems.

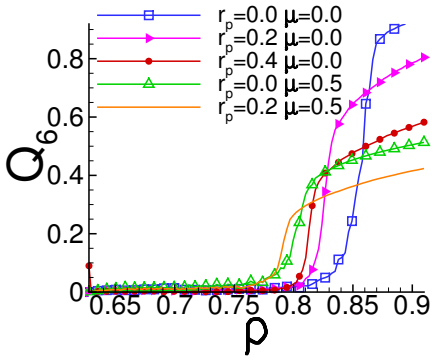

FIG. 8: (Color online) Order parameter showing distribution of the angles between contacts.

systems, we compute the pair correlation function, $g(r)$; the level of ordering of force networks is found from the force correlation function given by

$$g_f(r) = \frac{\sum_i \sum_{j>i} \delta\left(r_{ij} - r\right)\left(F_i - < F >\right)\left(F_j - < F >\right)}{\sum_i \sum_{j>i} \delta\left(r_{ij} - r\right)} \tag{10}$$

where F_i denotes the total normal force on i-th particle and r_{ij} is the distance between the particles i, j. Figure 7 shows $g(r)$ and $g_f(r)$, averaged over 120 realizations. We observe a pronounced first peak of $g(r)$ and $g_f(r)$ and a clearly split second peak, which is a sign of crystallization [35], for frictionless systems with $r_p = 0.0, 0.2$. For $\mu = 0.0$ and large polydispersity parameter, $r_p = 0.4$, and for frictional systems, the first peak of $g(r)$ and $g_f(r)$ is

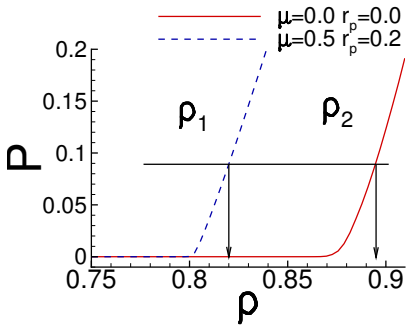

FIG. 9: (Color online) The pressure, P, on the the domain boundaries as a function of ρ for the reference and for $r_p = 0.0, \mu = 0.0$ system; ρ_1, ρ_2 correspond to the same pressure in reference and $r_p = 0.0, \mu = 0.0$ system, respectively.

less pronounced and clearly there is a smaller long-range correlation for both $g(r)$ and $g_f(r)$. We note that a choice of $r_p = 0.4$ for $\mu = 0.0$ guarantees that the system is not crystallized, and we can thus separate clearly the influence of the structural order and the influence of friction on our results.

Next we discuss Q_6, that measures the distribution of the angles between contacts, defined by

$$Q_6 = \frac{1}{N_p} \sum_i \frac{1}{C_i - 1} \sum_{k=1}^{C_i - 1} \cos(6\theta_k). \qquad (11)$$

Q_6 is a measure of the six-fold symmetry between contacts: here N_p is the total number of particles, C_i is the number of contacts for the i-th particle, and θ_k is the angle between two consecutive contacts. Note that Q_6 is equal to 1 for a perfect hexagonal crystal. Figure 8 shows the results averaged over all realizations. For small ρ's, Q_6 is small for all systems, but then, as the systems go through their respective jamming transitions, Q_6 grows. For $\rho > \rho_J$, we observe that the frictionless systems, in particular the monodisperse one, are the most ordered, consistently with the results obtained by considering $g(r)$ and $g_f(r)$. We also confirm our conclusion that the frictionless $r_p = 0.4$ system does not posses a structural order and is characterized by Q_6 that is similar to the ones found for the frictional systems.

To conclude this section, we find that frictionless systems that are built of strongly polydisperse particles do not lead to an ordered structure under slow compression. These systems, while disordered, lead to force networks that are non-universal in the sense that their fractal dimension, D_f, and the scaling exponent, ϕ, are not consistent. This being said, one could ask whether ordered frictional systems lead to universality. As suggested in the Introduction, this is not expected to be the case. To confirm this expectation, we carried out additional simulations where we arranged frictional particles on a hexagonal lattice and exposed them to the same compression protocol (figures not shown for brevity). We find that the simulations carried out with different system sizes produce inconsistent results, showing lack of universality, as expected.

The other scaling parameters for these systems are discussed further below in Sec. III E. Before that, we discuss some additional aspects related to the comparison of the scaling exponent ϕ and the fractal dimension.

D. Further discussion of the results for ϕ and the fractal dimension

Here we discuss briefly two effects that could potentially influence the results presented so far: non-vanishing compression rate, and the differences in ρ_J for the systems considered.

In [24], we showed that the compression speed influences percolation and jamming transitions, so it is appropriate to ask whether our scaling results are influenced by non-vanishing compression rate. For this reason, we also consider relaxed systems, where we stop the compression and relax the particles' velocities every $\Delta\rho = 0.02$, following the same protocol as presented in [24]. We then compute $1 + \phi$ and D_f using the same approach as discussed so far, and find that the values are consistent with the ones presented (figures not given for brevity). This finding is not surprising since here we focus on the systems above their jamming transitions. For such ρ's, consistently with the results given in [24], there does not seem to be any rate dependence of the results, at least for the slow compression considered here.

We further examine whether the inconsistency of the results for ϕ and D_f for the frictionless systems might arise from the proximity to the jamming transition. As noted above, ρ_J differs significantly between the considered systems, and it reaches particularly large values for the frictionless ones. Since we are comparing different systems, we need to confirm that they are all in the same regime, so sufficiently far away from ρ_J. As a measure, we consider here the (dimensionless) pressure, P (computed as the average force per length) on the domain boundaries. For the sake of brevity, we focus on two representative systems here, the reference one, and the $r_p = 0.0, \mu = 0.0$ system. Figure 9 shows P as a function of ρ for these two systems, averaged over all realizations. Since the reference system jams for much smaller ρ, P starts growing earlier. For definite comparison, consider a particular packing fraction, $\rho_1 = 0.82$ for the reference system: at this ρ, P is non-zero, and Fig. 6 and Table I show that ϕ and D_f are consistent. Consider now $r_p = 0.0, \mu = 0.0$ system at the packing fraction $\rho_2 = 0.895$ that corresponds to the same pressure. At this ρ, Fig. 6(c) shows inconsistent values of ϕ and D_f. We conclude that the difference in the results obtained from two different methods - scaling versus fractal dimension - for frictionless monodisperse system does not arise from the proximity to a jamming transition.

E. Continuation of the discussion of scaling parameters

We continue with the discussion of remaining scaling parameters, f_c and ν, found by minimizing err (the distance between the $\hat{S}$ curves) for different L's. Table I shows f_c and ν as a function of ρ for the considered frictional systems. While the value of f_c is almost constant, ν shows the same decreasing trend with increasing ρ for both considered frictional systems. We note, however, that the results for ν are different for monodisperse and polydisperse system: for the reference (polydisperse) case and sufficiently high ρ, we find $\nu \approx 1.5$, consistently with [20]. However, $r_p = 0.0, \mu = 0.5$ gives $\nu \approx 2$. Note also that for $r_p = 0.0$, $\mu = 0.5$ system and for $\rho = 0.82$ rather large err is found, suggesting larger inaccuracy in the (very) large optimal value of ν.

$r_p = 0.0$				
0.82	0.84	0.86	0.88	0.90
0.76	0.96	0.96	0.96	0.96
13.94	2.72	2.12	1.98	1.84
1.73	1.77	1.78	1.77	1.80
0.67	0.73	0.77	0.79	0.80
0.13	0.09	0.06	0.04	0.04

$r_p = 0.2$					
ρ	0.82	0.84	0.86	0.88	0.90
f_c	1.06	1.0	0.98	0.98	0.98
ν	1.68	1.7	1.54	1.48	1.38
D_f	1.78	1.80	1.79	1.78	1.81
ϕ	0.72	0.75	0.80	0.78	0.80
err	0.06	0.05	0.02	0.03	0.03

TABLE I: The results are shown for D_f, f_c and scaling exponent ν for the frictional systems; the value of err gives an estimate of the accuracy of the collapse.

$r_p = 0.0$				
0.88	0.885	0.89	0.895	0.90
0.22	0.56	0.60	0.66	0.54
13.96	8.76	6.84	5.48	6.52
1.70	1.71	1.73	1.74	1.75
0.81	0.82	0.86	0.89	0.87
0.02	0.02	0.01	0.01	0.01

$r_p = 0.2$				
ρ	0.84	0.86	0.88	0.90
f_c	1.18	1.1	1.08	1.06
ν	1.58	1.44	1.28	1.22
D_f	1.68	1.70	1.73	1.76
ϕ	0.77	0.78	0.80	0.84
err	0.01	0.01	0.08	0.01

$r_p = 0.4$					
ρ	0.82	0.84	0.86	0.88	0.90
f_c	1.34	1.08	1.08	1.04	1.04
ν	5.56	1.38	1.04	1.2	1.06
D_f	1.71	1.72	1.74	1.74	1.75
ϕ	0.85	0.85	0.85	0.82	0.85
err	0.08	0.1	0.07	0.07	0.07

TABLE II: The results are shown for D_f, f_c and scaling exponent ν for the frictionless systems; the value of err gives an estimate of the accuracy of the collapse.

Next we proceed with discussing the scaling exponents for frictionless systems. As an example, Fig. 10 shows err for the $r_p = 0.0$, $\mu = 0.0$ system at $\rho = 0.9$ (Fig. 4 shows the corresponding plots for the reference system). Direct comparison of these two figures shows the following: (i)

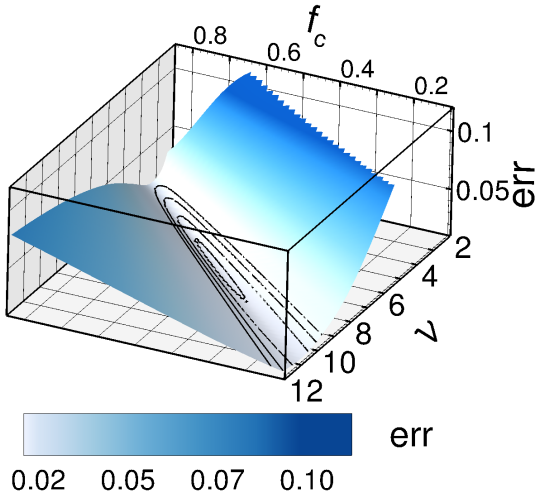

(a)

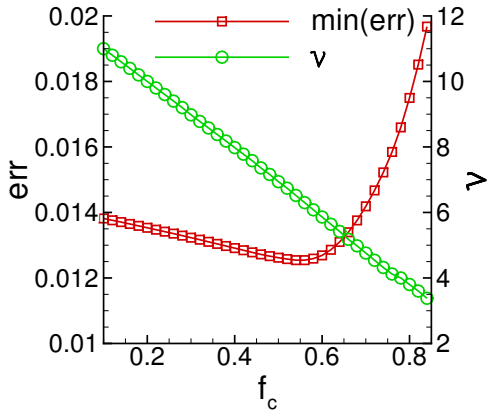

(b)

FIG. 10: (Color online) Error plot for the $r_p = 0.0, \mu = 0.0$ system at $\rho = 0.9$: (a) err as a function of f_c and ν; the black lines are slices through different values of err and (b) minimum of err (red line with squares) as a function of f_c; here for each f_c value we choose ν that minimizes err; the used values of ν are shown by the green line with circles. Note different range compared to Fig. 4.

the collapse appears to be much better for the considered frictionless system (the minimum value of err is smaller); (ii) the optimal values of f_c, ν are significantly different: ν is much larger, and f_c is much smaller for $r_p = 0.0$, $\mu = 0.0$ system. We note that the minimum of err curve in Fig. 10(b) is not as clearly defined as for the reference system, introducing some inaccuracy in the process of finding optimal values of f_c, ν. However, as it can be clearly seen in Fig. 10(b), this inaccuracy still limits f_c to a very small value, $f_c < 0.6$, and ν to a very large value, $\nu > 6$.

Figure 10 suggests some significant differences between $r_p = 0.0$, $\mu = 0.0$ and the reference system at $\rho = 0.9$.

Table II shows that the differences are present for other considered packing fractions as well. In particular, we always find large values of ν and very small values of f_c for $r_p = 0.0,\ \mu = 0.0$ system. Small overall values of err are a sign of a good quality of the collapse. We note again that for the smallest ρ, the optimal values of f_c and ν are different from the rest, suggesting that scaling properties of force networks very close to jamming transition may differ.

One obvious question to ask is what causes a particularly large difference between f_c and f_p for $r_p = 0.0,\ \mu = 0.0$ system (recall that typically $f_p \in [1.05, 1.25]$). One possibility is that it may be caused by a finite system size. Note that the percolation threshold in a finite size system, f_p, is related to the one of the infinite size system, f_p^∞, by [23]

$$|f_p - f_p^\infty| \sim L^{-1/\nu} \tag{12}$$

and $f_p^\infty < f_p$. This relation suggests a strong influence of the system size on f_p for large values of ν, such as those we are reporting in Table II for $r_p = 0.0,\ \mu = 0.0$ system. Therefore, our conjecture is that the agreement of f_c and f_p could still be found if very large system size are considered. In particular, if we assume that f_c is close to f_p^∞, the values of $f_c,\ f_p$ would be for a very large system both in the range $[0.5, 0.7]$ for $r_p = 0.0,\ \mu = 0.0$ system (see Table II).

We close this section by pointing out that ν could in principle be computed using alternative approaches. One avenue is to use Eq. (12); the value of f_p is found as an average percolation threshold for each L and plotted against the natural logarithm $\log(L^{-1/\nu})$; the slope of the linear fit should correspond to $-1/\nu$. However, we find that the error of the linear fit is large, leading to the results that are less accurate than the ones already obtained. Alternatively, we could estimate ϕ from the Fisher exponent τ, see Eq. (4), and the relation $\phi = (3-\tau)/(\tau-1)$. The results for ϕ obtained in this manner are again characterized by large error bars. We note that while both of the outlined approaches lead to the results that are inaccurate, they are still consistent with the ones found by scaling.

F. Physical experiments: ϕ and the fractal dimension

In this section we report the results of physical experiments carried out with photoelastic particles, made from the PSM-1 sheets obtained from Vishay Precision Group; details about the material properties of these particles could be found in [36]. Figure 1 shows the experimental setup that consists of two plexiglass plates with a thin gap in between. The size of the gap is slightly larger than the thickness of the particles. The domain is bounded by four walls, one of which is removable and can slide in and out. The experimental protocol consists of placing

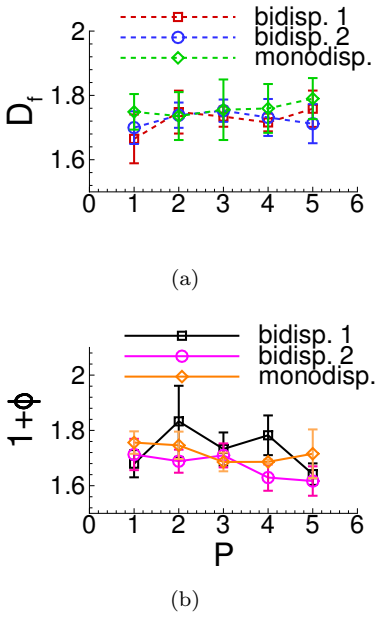

FIG. 11: (Color online) (a) Fractal dimension, D_f, and (b) $1+\phi$ obtained from experiments carried out with photoelastic particles, as a function of the applied pressure. Bidisperse 1 and 2 refer to the systems of large/medium and large/small particles, respectively (see the text).

the particles in the gap, mixing them up, and than replacing the removable wall and gently applying desired pressure by a certain number (1 - 5) of rubber bands. The applied pressures lead only to modest inter-particle forces. For each pressure, 5 realizations are carried out.

The stress on the particles is visualized using cross-polarizers (see Fig. 1(b)). The photographs are processed using the Hough Transform [37] image processing technique to detect particles. From the brightness of the particles, the total stresses are computed via G^2 method used extensively by Behringer's group (see, e.g. [38]). The experiments are carried out using three particle sizes of diameters 0.58, 0.46 and 0.41 cm. We consider a monodisperse system (with medium particles only) and two bidisperse ones that use large/medium and large/small particles. For bidisperse systems, we always use equal area fraction of particles of different sizes. Approximately $1,000$ particles are used in total.

The obtained data are processed similarly to the ones resulting from the simulations, with the difference that here we focus on the magnitude of the total stress on a particle, instead on contact forces, as in simulations. Since only a single domain size is available, the domain is divided into 4, 8 and 16 smaller sub-domains of $1/4, 1/8$ and $1/16$ of the original domain size. D_f and ϕ are then computed using the box-counting method and by fitting the peaks of S-curves, respectively. In what follows we focus on these two quantities only, since they could be obtained with a reasonable accuracy using available re-

sources.

Figure 11 shows D_f and $1+\phi$ computed from the experimental data. We note that while D_f is consistent for the whole range of pressures applied and for all experimental setups, the value of $1+\phi$ has a larger variation, similarly as for the results obtained from the simulations. Since the number of realizations used for the experiments is much smaller, relatively large standard error is observed in the results. Still, the experiments yield D_f and ϕ that are consistent with the results obtained from the simulations carried out with frictional particles. This is encouraging, in particular since the protocols in simulations and experiments differ (e.g., controlled pressure versus controlled packing fraction, additional friction between the particles and the substrate in experiments, that is not present in simulations); in addition, we have not attempted to precisely match the simulation parameters with material properties of the particles. The consistency of the results therefore suggests that they are independent of the protocol and of the material properties, at least for the applied pressures considered. We emphasize in particular that both simulation and experimental results lead to D_f and ϕ that are significantly smaller than the previously proposed value of $\phi \approx 0.9$ [20].

IV. CONCLUSIONS

In this paper we focus on the scaling properties of force networks in compressed particulate systems in two spatial dimensions. To complement the results obtained by exploring scaling properties of the force networks, we also calculate the fractal dimension. For disordered frictional systems, we find that the scaling exponent, ϕ, and the fractal dimension, D_f, are consistent over a range of considered packing fractions, ρ. The computed values are, however, significantly lower than the previously proposed ones, and in particular we find that $D_f \approx 1.8$. This value is consistent with the ones extracted from the physical experiments involving two dimensional systems of monodisperse and bidisperse frictional particles exposed to compression. We note that the reported experimental results are based on stresses, and not on the contact forces; it would be very much of interest to carry out additional experiments where individual contact forces would be resolved, and compare the results to the findings reported here.

Another significant finding is that the proposed universality of the force networks does not appear to hold for frictionless systems: in particular, for such systems the results for the scaling exponent, ϕ, and the fractal dimension, D_f, are not consistent. By considering strongly polydisperse frictionless systems that do not crystallize, we show that it is friction itself, and not partial crystallization (alone) that breaks universality. Therefore, we show that frictionless systems do not belong to the same (if any) universality class as the frictional ones. This being said, we have also shown that partial structure (that appears spontaneously for frictionless systems with sufficiently small range of the particle sizes, or can be induced 'by hand' for frictional ones) also leads to breakup of universality: therefore, *both friction and disorder are needed for force networks to show universality.*

These results open new directions of research, including working towards understanding the conditions under which scaling properties of force networks are at least consistent if not universal. Another question is how our findings extend to three dimensional systems. And finally, how the scaling properties of the force networks relate to the macroscopic properties of the underlying physical systems.

Acknowledgments The authors thank Robert Behringer and Mark Shattuck for the help with the experimental setup and many useful discussions. The experimental results were obtained and processed by a group of undergraduate students (class of 2012) supervised by Te-Sheng Lin and the authors. This work was supported by the NSF Grants No. DMS-0835611 and DMS-1521717.

[1] R. Albert and A.-L. Barabási, Rev. Mod. Phys. **74**, 47 (2002).
[2] S. Alexander, Phys. Rep. **296**, 65 (1998).
[3] D. M. Mueth, H. M. Jaeger, and S. R. Nagel, Phys. Rev. E. **57**, 3164 (1998).
[4] F. Radjai, J. J. Moreau, and S. Roux, Chaos **9**, 544 (1999).
[5] F. Radjai, D. E. Wolf, M. Jean, and J.-J. Moreau, Phys. Rev. Lett. **80**, 61 (1998).
[6] T. S. Majmudar and R. P. Behringer, Nature **435**, 1079 (2005).
[7] L. E. Silbert, Phys. Rev. E **74**, 051303 (2006).
[8] J. Wambaugh, Phys. D **239**, 1818 (2010).
[9] J. Peters, M. Muthuswamy, J. Wibowo, and A. Tordesillas, Phys. Rev. E **72**, 041307 (2005).
[10] A. Tordesillas, D. M. Walker, and Q. Lin, Phys. Rev. E **81**, 011302 (2010).
[11] A. Tordesillas, D. M. Walker, G. Froyland, J. Zhang, and R. P. Behringer, Phys. Rev. E **86**, 011306 (2012).
[12] D. S. Bassett, E. T. Owens, K. E. Daniels, and M. A. Porter, Phys. Rev. E **86**, 041306 (2012).
[13] M. Herrera, S. McCarthy, S. Slotterback, E. Cephas, W. Losert, and M. Girvan, Phys. Rev. E **83**, 061303 (2011).
[14] D. M. Walker and A. Tordesillas, Phys. Rev. E **85**, 011304 (2012).
[15] R. Arévalo, I. Zuriguel, and D. Maza, Phys. Rev. E **81**, 041302 (2010).
[16] R. Arévalo, L. A. Pugnaloni, I. Zuriguel, and D. Maza, Phys. Rev. E **87**, 022203 (2013).
[17] L. Kondic, A. Goullet, C. O'Hern, M. Kramar, K. Mischaikow, and R. P. Behringer, Europhys. Lett. **97**, 54001

(2012).
[18] M. Kramar, A. Goullet, L. Kondic, and K. Mischaikow, Phys. Rev. E **87**, 042207 (2013).
[19] M. Kramar, A. Goullet, L. Kondic, and K. Mischaikow, Phys. Rev. E **90**, 052203 (2014).
[20] S. Ostojic, E. Somfai, and B. Nienhuis, Nature **439**, 828 (2006).
[21] S. Ostojic, T. J. H. Vlugt, and B. Nienhuis, Phys. Rev. E **75** (2007).
[22] R. Pastor-Satorras and M.-C. Miguel, J. of Stat. Mech. **2012** (2012).
[23] D. Stauffer and A. Aharony, *Introduction to Percolation Theory* (CRC Press, 1994).
[24] L. Kovalcinova, A. Goullet, and L. Kondic, Phys. Rev. E **92**, 032204 (2015).
[25] J. Geng, R. P. Behringer, G. Reydellet, and E. Clément, Phys. D **182**, 274 (2003).
[26] L. Kondic, Phys. Rev. E **60**, 751 (1999).
[27] P. A. Cundall and O. D. L. Strack, Géotechnique **29**, 47 (1979).
[28] L. Brendel and S. Dippel, in *Physics of Dry Granular Media*, edited by H. J. Herrmann, J.-P. Hovi, and S. Luding (Kluwer Academic Publishers, Dordrecht, 1998), p. 313.
[29] C. Goldenberg and I. Goldhirsch, Nature **435**, 188 (2005).
[30] D. Blair, N. Mueggenburg, A. Marshall, H. Jaeger, and S. Nagel, Phys. Rev. E **63**, 413041 (2001).
[31] A. R. T. van Eerd, W. G. Ellenbroek, M. van Hecke, J. H. Snoeijer, and T. J. H. Vlugt, Phys. Rev. E **75**, 060302 (2007).
[32] D. Bi, J. Zhang, B. Chakraborty, and R. P. Behringer, Nature **480**, 355 (2011).
[33] J. Zhang, T. S. Majmudar, M. Sperl, and R. P. Behringer, Soft Matter **6**, 2982 (2010).
[34] X. Cheng, Phys. Rev. E **81**, 031301 (2010).
[35] T. M. Truskett, S. Torquato, S. Sastry, P. G. Debenedetti, and F. H. Stillinger, Phys. Rev. E **58**, 3083 (1998).
[36] A. H. Clark, A. J. Petersen, L. Kondic, and R. P. Behringer, Phys. Rev. Lett. **114**, 144502 (2015).
[37] R. O. Duda and P. E. Hart, Commun. ACM **15**, 11 (1972).
[38] A. H. Clark, L. Kondic, and R. P. Behringer, Phys. Rev. Lett. **109**, 238302 (2012).